

Technique for Simultaneously Measuring Fluctuating Velocity, Temperature and Concentration in Non-isothermal Flow

Ryuichiro Yoshie^a, Hideyuki Tanaka^a, Taichi Shirasawa^a

^aTokyo Polytechnic University, 1583, Iiyama, Atsugi, Kanagawa, Japan

ABSTRACT: In this study, we aimed to provide experimental data to validate CFD for pollutant diffusion around buildings in non-isothermal flow. We developed a system for simultaneously measuring fluctuating velocity, temperature and concentration. The system compensates for the contribution of temperature to output voltage of a split film with a cold wire. We made a calibrator for a split film for different temperatures and proposed calibration equations for it, and it showed good performance. These equations can be used to simultaneously measure wind velocity and temperature around buildings in non-isothermal flow. We used a high speed flame ionization detector to measure concentration simultaneously with wind velocity and temperature, enabling us to provide turbulence statistics such as heat flux and concentration flux.

KEYWORDS: Non-isothermal flow, Pollutant diffusion, Heat flux, Concentration flux

1 INTRODUCTION

Computational Fluid Dynamics (hereinafter abbreviated as “CFD”) is expected to become a useful means for predicting and evaluating the wind environment, heat island phenomena, and pollutant diffusion in urban areas. For CFD to be developed as a more practical prediction tool, it is indispensable to examine its prediction accuracy by field measurements or wind tunnel experiments. In wind tunnel experiments that target pollutant diffusion or heat island phenomena in a non-isothermal flow in urban areas influenced by solar and nocturnal radiations, wind velocity is usually measured using a Laser Doppler Velocimeter (LDV), which is not influenced by air temperature¹⁾. However, this gives rise to the possibility of seeding particles affecting the sensors and instruments for measuring temperature and pollutant concentration, making it difficult to measure wind velocity, temperature, and pollutant concentration simultaneously. In some experiments, wind velocity and temperature have been measured by combining an X probe and a cold wire, but their targets have been limited to a stable atmospheric boundary layer²⁾ and a flow field over a two-dimensional low hill³⁾ with no reverse flow. This is because the X probe cannot distinguish positive flow from negative flow when there are considerable velocity fluctuations. This paper describes a measurement technique developed by the authors to deal with the “non-isothermal flow field around buildings” where measurement is extremely difficult.

With this technique, the measurement system is composed of a split film (S.F.), a cold wire (C.W.), and a high speed flame ionization detector (FID), and enable the following:

- Simultaneous measurement of instantaneous wind velocity, temperature, and concentration.
- Measurement of a flow field with a large turbulence intensity accompanied by positive and negative (reverse) flows.
- Appropriate temperature compensation for a flow with a large temperature fluctuation.

In order to improve the calibration precision of the split film and the cold wire, calibrators for the hot and cold wires were used, and calibration equations were proposed for temperature compensation for the split film. In addition, the measurement precision was controlled by analyzing measurement uncertainty⁴⁾, and the uncertainty of measurement results was evaluated in order to improve the reliability of the experimental results as data for validating CFD.

2 CALIBRATOR FOR HOT AND COLD WIRES

2.1 Outline of calibrator

In order to precisely compensate for the contribution of temperature fluctuation to the output voltages of the split film under the low wind speed condition, it is necessary to obtain precise calibration data under the stable wind speed and temperature condition. In this experiment, a calibrator for a hot-wire anemometer and a cold-wire thermometer (Fig. 1) was used to improve calibration precision and efficiency.

In this calibrator, a laminar flow-meter measures the flow volume rate inside the calibrator (diameter: $D = 100$ mm), and the cross section mean wind speed U_{mean} is obtained by dividing the flow volume rate by the area of cross section at the measurement point. Based on this U_{mean} and the wind speed distribution shown in Fig. 2 (discussed later), calibrated wind speed U_c (wind speed at the center of the calibrator) is obtained. For temperature control inside the calibrator, a duct heater was used, and the air temperature θ_a inside the calibrator was measured with a thermocouple with a wire diameter of $75 \mu\text{m}$. Here, heat insulating material was used for outer package, to reduce the influence of the air temperature outside the calibrator.

2.2 Features of calibrator

Fig. 2 shows the wind speed and temperature distributions inside the calibrator. They were both homogeneous around the center of the calibrator ($Z/(D/2) = 0$). If a hot wire and a cold wire are placed around the center of the calibrator, the influence of error on calibration precision is extremely small. Fig. 3 shows the turbulence intensities of wind speed and air temperature at $Z/(D/2) = 0$. They were both very small: $I_u < 1\%$, $I_\theta < 2\%$. Fig. 4 shows the relative uncertainty, $U_e(U_c)/|U_c|$, of wind speed of this calibrator which was less than 1.5%. However, when a wind tunnel was used instead of the calibrator, it was about 5.0%. Thus, the calibrator greatly improved the credibility of the wind speed. The relative uncertainty of temperature $U_e(\theta_a)/|\theta_a|$ showed no significant differences, being less than 1.5% in both cases.

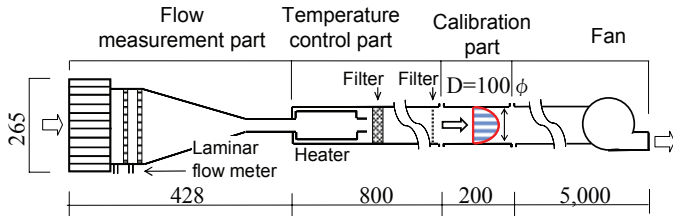


Figure 1. Calibrator for hot-wire and cold-wire

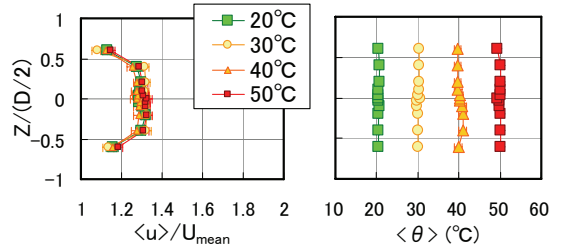
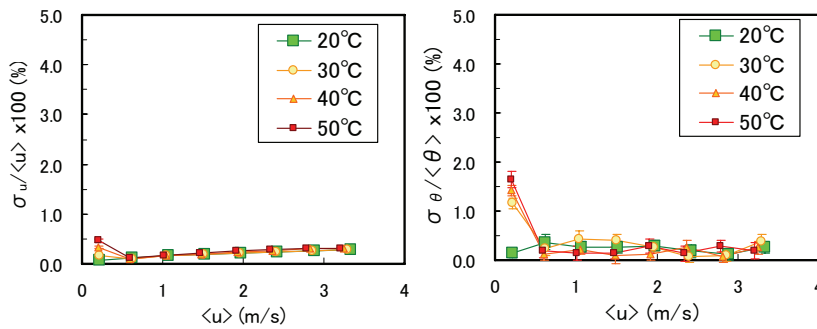


Figure 2. Distribution inside calibrator



(a) $\sigma_u / \langle u \rangle$ (b) $\sigma_\theta / \langle \theta \rangle$

Figure 3. Turbulence intensity

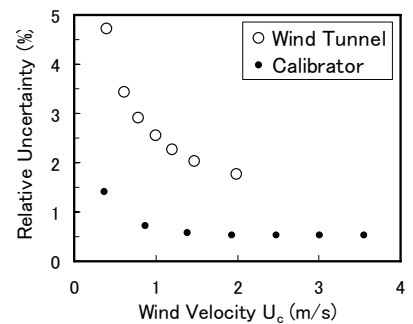


Figure 4. Relative uncertainty (Wind velocity for calibration)

3 CALIBRATION OF COLD WIRE AND SPLIT FILM

In this measurement system, a split film of DANTEC (55R55) and CTA Module (90C10) were adopted for wind velocity measurement; and a cold wire (55P31) and Temperature Module (90C20) were used for temperature measurement. These sensors were placed at about 5-mm intervals so that the split film and the cold wire do not affect to each measured value. The procedures for obtaining calibration data are as follows:

- 1) The angle of the wind approaching the split film is set as $\alpha = 0^\circ$ (Fig. 5) under a constant air temperature, wind speed U_c is changed in 8 ways. For each wind speed, the split film's output voltages E_1, E_2 are measured, and air temperature θ_a by the thermocouple and output voltage E_{cw} from the cold wire are measured.
- 2) The angle of the wind approaching the split film is set as $\alpha = 180^\circ$, and the above mentioned measurements are repeated.
- 3) The above procedures are conducted for several air temperatures (10 °C - 60 °C), to obtain $\theta_a, E_1, E_2, E_{cw}$ for each temperature.

3.1 Calibration of cold wire (C.W.) and measurement of air temperature

Fig. 6 shows the relation between air temperature θ_a measured by the thermocouple and output voltage E_{cw} from the cold wire in the calibrator. As shown, E_{cw} does not depend on wind speed. The linear function is obtained by the least square method based on the measurement data θ_a and E_{cw} shown in Fig.6, and then the calibration coefficients A_c and B_c are obtained from equation (1).

In wind tunnel experiments, the instantaneous air temperature θ_a is calculated from the measured E_{cw} and the calibration coefficients A_c and B_c by using equation (1):

$$E_{cw} = A_c + B_c \theta_a \quad (A_c \text{ and } B_c \text{ are constant}) \quad (1)$$

3.2 Calibration of split film (S.F.) and measurement of wind velocity components

3.2.1 Calibration of split film (S.F.)

Fig. 7 shows the relation between air temperatures θ_a measured by the thermocouple and output voltage $E_1^2 + E_2^2$ from the split film in the calibrator. The sensor part of the split film is kept at a fixed high temperature θ_s . As air temperature θ_a increases, the difference between θ_a and θ_s becomes smaller, and the convective heat transfer from the split film to air decreases, and so the output voltages E_1 and E_2 from the split film become lower. Equation(2) is obtained from this reason. The intercept of the first-order approximation formula, obtained from the least square method using this relation, corresponds to the sensor part temperature θ_s .

$$\langle \theta_a \rangle = \theta_s + C (\langle E_1 \rangle^2 + \langle E_2 \rangle^2) \quad (C \text{ is constant}) \quad (2)$$

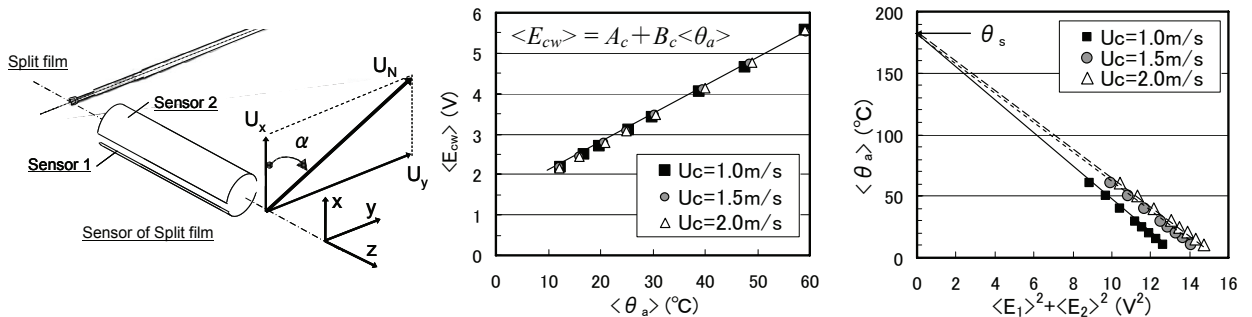


Figure 5. Definition coordinates of S.F. Figure 6. Relation between θ_a and E_{cw}

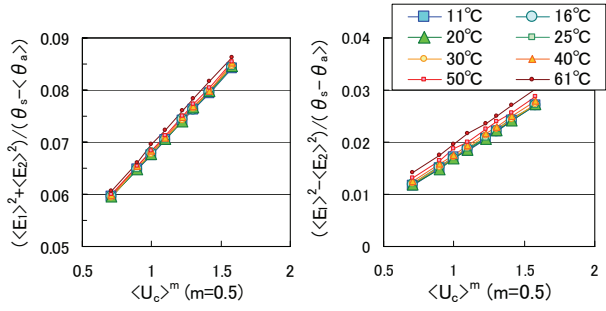
Figure 7. Relation between θ_a and θ_s

The relation between the split film's output voltages E_1 and E_2 and the calibrated wind speed U_c is evaluated from the following equations based on King's law.

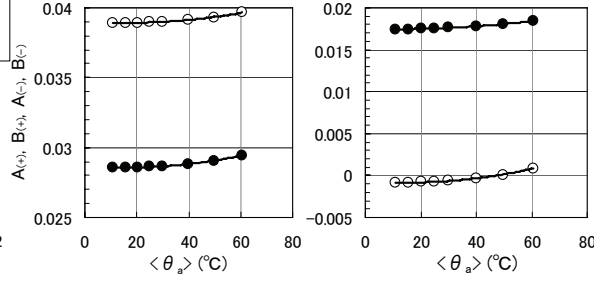
$$\frac{\langle E_1 \rangle^2 + \langle E_2 \rangle^2}{\theta_s - \langle \theta_a \rangle} = A_{(+)} + B_{(+)} \langle U_c \rangle^m \quad (3),$$

$$\frac{\langle E_1 \rangle^2 - \langle E_2 \rangle^2}{\theta_s - \langle \theta_a \rangle} = A_{(-)} + B_{(-)} \langle U_c \rangle^m \quad (4)$$

In Fig. 8(a) and (b), the vertical axes represent the left-hand sides of equations (3) and (4), respectively, and the horizontal axes depict $\langle U_c \rangle^m$. The value of m was specified so that the data can be best approximated by a linear function. In this calibration, $m = 0.5$. As shown in Fig. 8, since the calibration curves are influenced by air temperature θ_a , the calibration coefficients $A_{(+)}$, $B_{(+)}$, $A_{(-)}$, $B_{(-)}$ become functions of θ_a , as shown in Fig. 9. Here, these coefficients are approximated by quadratic functions.



(a) Sum of squares (b) Difference of squares
Figure 8. Calibration curves



(a) Sum of squares (b) Difference of squares
Figure 9. Calibration coefficients $A_{(+)}$, $B_{(+)}$, $A_{(-)}$, $B_{(-)}$

3.2.2 Measurement of wind velocity components U_x , U_y

Fig. 10 shows the characteristics of the split film's output voltages E_1 and E_2 when the angle α of the wind approaching the split film is changed (Refer to Fig.5).

The wind velocity's calibration coefficients $A_{(+)}$, $B_{(+)}$, $A_{(-)}$, $B_{(-)}$ are calculated from the instantaneous air temperature θ_a obtained in 3.2.1, and these calibration coefficients are used to compensate for the contribution of temperature fluctuations to the split film's output voltages E_1 and E_2 . The conversion to instantaneous scalar wind velocity U_N is obtained from:

$$\frac{E_1^2 + E_2^2}{\theta_s - \theta_a} = A_{(+)} + B_{(+)} U_N^m \quad (5)$$

As shown in Fig. 10(b), the squared difference of the split film's output voltages C_a (Eq.(7)) can be approximated by a cosine curve, and so the instantaneous value of α is evaluated from:

$$\alpha = \begin{cases} \cos^{-1} \frac{C_a - C_{90}}{|C_0 - C_{90}|} & \text{(in the case of positive flow } (C_a - C_{90} \geq 0)) \\ \cos^{-1} \frac{C_a - C_{90}}{|C_{180} - C_{90}|} & \text{(in the case of negative (reverse) flow } (C_a - C_{90} < 0)) \end{cases} \quad (6)$$

where

$$C_a = \frac{E_1^2 - E_2^2}{\theta_s - \theta_a} \quad \text{(vertical axes in Fig. 8 (b) and Fig. 10 (b))} \quad (7)$$

$$C_0 = A_{(-),0} + B_{(-),0} U_N^m \quad (8)$$

$A_{(-),0}$, $B_{(-),0}$: calibration coefficients $A_{(-)}$, $B_{(-)}$ at $\alpha = 0^\circ$

$$C_{180} = A_{(-),180} + B_{(-),180} U_N^m \quad (9)$$

$A_{(-),180}$, $B_{(-),180}$: calibration coefficients $A_{(-)}$, $B_{(-)}$ at $\alpha = 180^\circ$

$$C_{90} = (C_0 + C_{180})/2 \quad (10)$$

In the sum of squares of the split film's output voltages, there are differences of about 5% among the cases of $\alpha = 0^\circ$, 180° , and 90° , as shown in Fig. 10(a), and so equation (5) is also a function of α . Therefore, in this calibration method, U_N and α that satisfy both equations (5) and (6) are calculated using an iteration method.

Using the instantaneous values of U_N and α , obtained from the above calibration equations, the instantaneous values of wind velocity components U_x and U_y are evaluated from:

$$U_x = U_N \cos \alpha \quad (11), \quad U_y = U_N \sin \alpha \quad (12)$$

The scaler wind velocity U_N measured with this calibration method and the measurement U by the ultrasonic anemometer are compared in Fig. 11. In addition, Fig. 12 shows the measured value of $(C_\alpha - C_{90}) / (C_{0,180} - C_{90})$ against the wind angle α . Both U_N and α were measured precisely, and their relative uncertainties were below 5%.

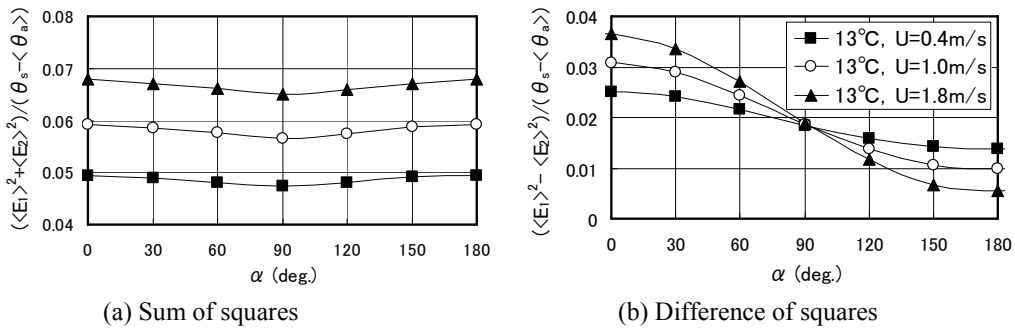


Figure 10. Characteristics of split film's output voltages

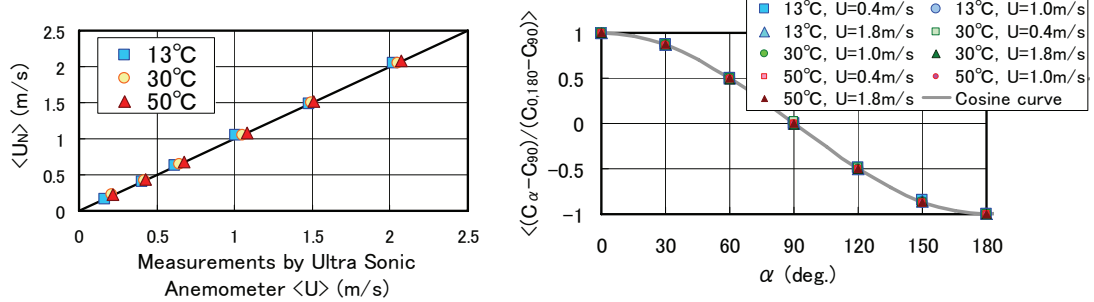


Figure 11. Calibration accuracy of U_N Figure 12. Calibration accuracy of $(C_\alpha - C_{90}) / (C_{0,180} - C_{90})$

4 EFFECTS OF LAYOUT OF SENSORS ON MEASURED VALUES

In this system, it is necessary to place a split film, a cold wire, and a sampling tube of a high-speed flame ionization detector (FID) adjacent to one another. The effects of this layout on measured values were studied. For the measurement, the thermally stratified wind tunnel (cross section of the measurement part: $1.2 \text{ m} \times 1.0 \text{ m}$) of Tokyo Polytechnic University was used. The sampling frequency and the low-pass filter's cutoff frequency were set at 1000 Hz and 200 Hz, respectively, and 120,000 data were sampled in 120 seconds. For the FID, a sampling tube with an inner diameter of 0.25 mm and a length of 300 mm was adopted, and the aspiration rate and time constant were specified to be 17.9 m/s and 14.7 ms, respectively.

4.1 Effects on mean wind velocity and mean temperature

The effects of a layout of sensors on the measured value of each sensor were studied. The center of a reference sensor is assumed as the origin, and measurement was carried for varying distances between the origin and each sensor. The directions of the distance were the x, y

and z directions (Refer to Fig. 5). The measurement point was within the turbulent boundary layer (unstable stratification with $\theta_a = 10^\circ\text{C}$, $\theta_f = 50^\circ\text{C}$), and measurement was conducted at a height where turbulence intensity $I_u = 0.10$ and 0.25 . The measured values at each height are tabulated in Table 1. For the FID which was placed in the y direction of the split film, U_N decreased by about 0.05 m/s (Fig. 13(a), left). For $I_u = 0.10$, when the FID was placed at $\Delta x = 2$ mm (Fig. 13(a), left), U_N increased slightly, and so there is a possibility that the aspiration rate of the FID produced some influence on velocity measurement. As shown in Fig. 13 (b), under the condition of this measurement, the temperature ($\approx 180^\circ\text{C}$) of the sensor part of the split film has little influence on the cold wire.

Exp. Case	$I_u=0.10$	$I_u=0.25$
Measured height Z (m)	0.03	0.01
$\langle U_N \rangle$ (m/s)	1.24	0.82
σ_{U_N} (m/s)	0.12	0.20
$\langle \theta_a \rangle$ ($^\circ\text{C}$)	21.7	17.1
σ_{θ_a} ($^\circ\text{C}$)	1.51	2.51
$\langle c \rangle$ (ppm)	604	716
σ_c (ppm)	349	1231

4.2 Effects on heat and concentration fluxes

The center of the split film's sensor part is assumed as the origin, and measurement was carried for varying distances between the origin and the cold wire or FID. The directions of the distance

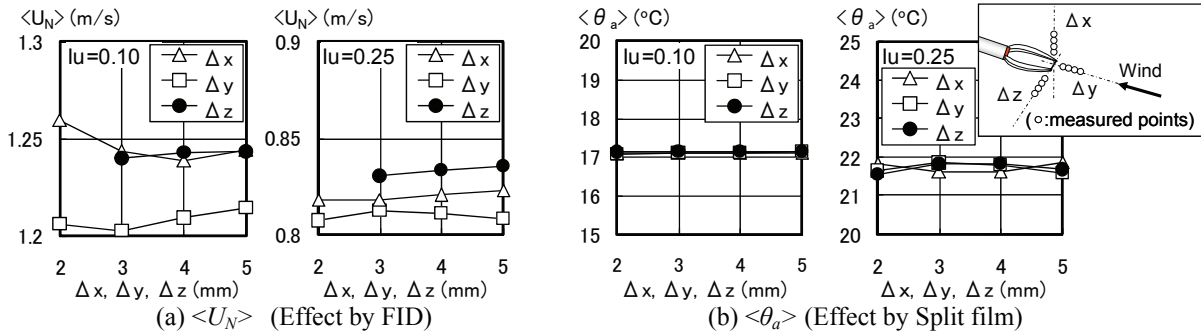


Figure 13. Effects of layout of sensors on measured values

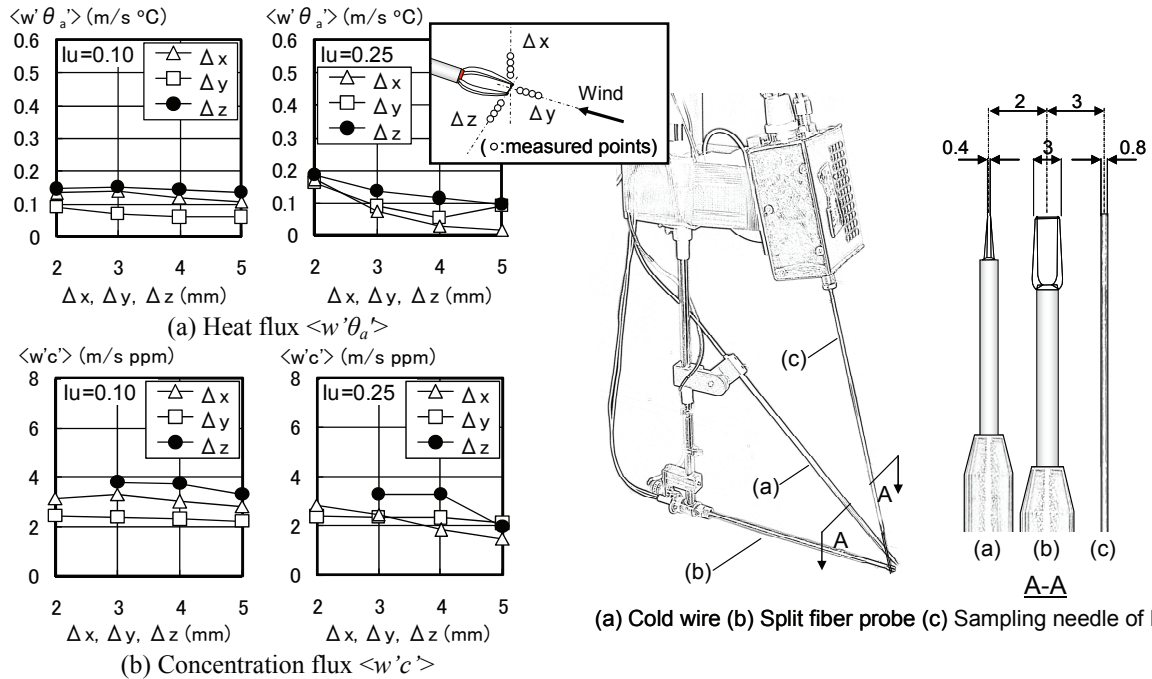


Figure 14. Effects of layout of sensors on measured fluxes

Figure 15. Layout of sensors

change were the x, y and z directions (Refer to Fig.5). Fig. 14 shows $\langle w'\theta_a' \rangle$ and $\langle w'c' \rangle$. For both $I_u = 0.10$ and 0.25 , the heat flux depended more on the distance Δ when the cold wire was placed in the x or y direction than when it was placed in the z direction (Fig. 14(a)). For $I_u = 0.10$, the heat flux was almost constant when $\Delta z \leq 4$ mm (Fig. 14(a), left). The concentration flux in Fig. 14 (b) is almost constant in the range of $\Delta y, \Delta z \leq 4$ mm, for both $I_u = 0.10$ and 0.25 .

Therefore, there is a possibility that the other sensor placed in the x and y direction would affect the measured wind velocities. Therefore, in this experiment, the cold wire was placed at the position $\Delta z = 2$ mm and the FID was placed at the position $\Delta z = 3$ mm, as shown in Fig. 15. In addition, the uncertainties of the measured heat fluxes and concentration fluxes caused by the distance between sensors were evaluated with $\partial\langle w'\theta_a' \rangle/\partial z$ and $\partial\langle w'c' \rangle/\partial z$ being sensitivity coefficients.

5 EXAMPLE OF MEASUREMENT IN FLOW FIELD INCLUDING REVERSE FLOW

5.1 Overview of experiment

This section describes a measurement example of a flow field including reverse flow behind the a two-dimensional fence in a non-isothermal boundary layer, using this measuring technique. The target flow field and coordinates are shown in Fig. 16, and the air flow conditions are tabulated in Table 2. For this experiment, the thermally stratified wind tunnel of Tokyo Polytechnic University was used. The two-dimensional fence was modeled by an aluminum plate 100 mm high and 5 mm thick with its upper edge cut at a 45° angle, placed perpendicular to the flow ($U_\delta = 1.6$ m/s). Tracer gas (C_2H_4) was released at a flow rate $Q = 0.6$ l/min from a hole ($\phi=5$ mm) on the floor behind the fence. In this measurement, when the u component of wind velocity was measured, the direction of the split film was set as $U_x = u$, and when the w component was measured, it was set as $U_x = w$ (Refer to Fig.5, for the U_x component). In order to measure pollutant concentration, it is necessary to allocate sufficient time for averaging, and so 120-sec measurement was conducted at a sampling frequency of 1,000 Hz. The cutoff frequency of the low-pass filter was 200 Hz.

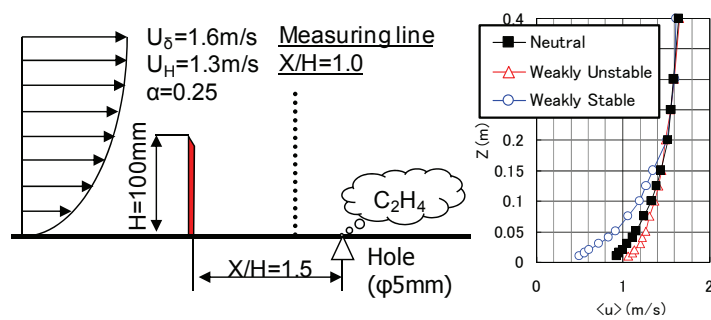


Figure 16. Target Flow Field

Table2 Condition of Wind tunnel

Exp. case	Neutral	Weakly Unstable	Weakly Stable
δ (m)	0.30	0.30	0.30
$\langle \theta_r \rangle$ ($^{\circ}$ C)	12.73	42.57	19.00
$\langle \theta_\delta \rangle$ ($^{\circ}$ C)	12.05	12.88	51.67
$\langle \theta_0 \rangle$ ($^{\circ}$ C)	12.16	21.23	37.68
$\langle U_\delta \rangle$ (m/s)	1.62	1.62	1.62
R_b	0.00	-0.11	0.12

Bulk Richardson number:

$$R_b = g\delta(\theta_\delta - \theta_0) / \{(\theta_0 + 273)(U_\delta^2)\}$$

5.2 Measurement results

Fig. 17 shows the vertical distribution of mean wind velocity, temperature, concentration, and fluxes at $X/H = 1.0$ downstream of the two-dimensional fence. As shown in Fig. 17(a), it is possible to distinguish positive flow from negative (reverse) flow. From the analysis of uncertainties of heat and concentration fluxes shown in Fig. 17(d) and (e), the uncertainty for the weakly unstable case was larger than that for other cases due to the strong turbulence.

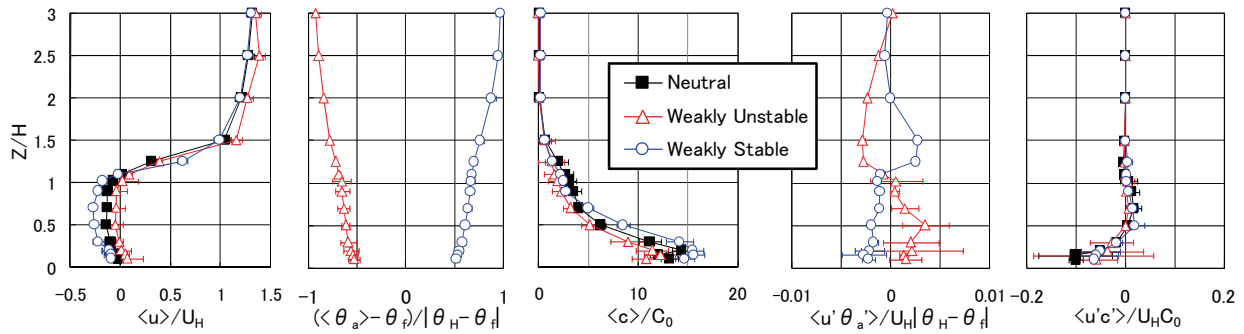


Figure 17. Vertical Profiles of Experimental Result

6 SUMMARY

With the purpose of measuring the flow around buildings under the non-isothermal condition, the authors developed a system for simultaneously measuring wind velocity, temperature, pollutant concentration, and proposed a calibration method. The findings of this paper are summarized as follows:

- 1) The turbulence intensities I_u and I_θ of wind velocity and temperature inside the developed calibrator for hot and cold wires were less than 1% and less than 2%, respectively ($I_u < 1\%$, $I_\theta < 2\%$). Therefore, this calibrator can supply air with stable velocity and temperature.
- 2) When a cold wire is placed in the direction of the split film sensor axis (z direction in Fig.5), the heat flux is not strongly influenced by the distance between the split film and the cold wire.
- 3) If the interval between the split film and the FID is less than 4 mm in the direction of the split film sensor axis (z direction in Fig.5), the uncertainties of concentration flux due to different sensor positions become smaller.
- 4) With the proposed calibration equations for the split film, it becomes possible simultaneously to measure wind velocity and temperature of flow around buildings under the non-isothermal condition. In addition, unlike LDV, seeding particles are not used, and so it is possible to measure pollutant concentration simultaneously with velocity and temperature.
- 5) With this measurement system, it is possible to measure the mean and fluctuations of the three components of wind velocity, temperature and pollutant concentration, as well as heat flux and concentration flux.

[Symbols]

X, Y, Z	: Space coordinates (main flow, transverse, and vertical directions in the wind tunnel)	U_x, U_y	: wind velocity components acting on S.F. (Refer to Fig.5)
x, y, z	: S.F. coordinates (Refer to Fig.5)	α	: angle of wind approaching (Refer to Fig.5)
$\langle \zeta \rangle$: time averaged variable ζ	θ_a, θ_H	: air temperature, air temperature at fence height
ζ'	: variation of variable ζ ($= \zeta - \langle \zeta \rangle$)	θ_s	: temperature of the S.F. sensor
σ_ζ	: standard deviation of variable ζ	θ_f	: surface temperature of wind tunnel floor
$U_\zeta(\zeta)$: expanded uncertainty of variable ζ ⁴⁾	θ_θ	: mean air temperature inside the boundary layer
u, v, w	: three components of wind velocity	c	: tracer gas concentration
U_δ, U_H	: wind speed, wind speed at fence height	Q	: tracer gas flow rate
U_{mean}	: cross-sectional mean wind speed in the calibrator	C_0	: reference concentration, $C_0 = Q / (U_H \cdot H^2)$
U_c	: reference wind speed for calibration	H, δ	: reference height, boundary layer height
U_N	: scalar wind velocity	E_1, E_2	: measured voltage of S.F.
		E_{cw}	: measured voltage of C.W.

7 REFERENCES

- 1) K. Uehara, S. Murakami, S. Oikawa, S. Wakamatsu, Wind Tunnel Test on Stratified Flow Fields around Urban Street Canyons by LDV, *J. Archit. Plann. Environ. Eng., AIJ*, No.492, pp.39-46, 1997
- 2) Y. Ohya, Wind Tunnel Study of Atmospheric Stable Boundary Layers over a Rough Surface, *Boundary-Layer Meteorology*, Vol.98, pp.57-82, 2001
- 3) R. Zegadi, M. Ayarault, P. Mejean, Effect of a Two-dimensional Low Hill in a Thermally Neutral and Stable Stratified Turbulent Boundary Layer, *Atmospheric Environment*, Vol.28, No.11, pp.1871-1878, 1994
- 4) ISO, Guide to the Expression of Uncertainty in Measurement, 1993